Effect of Loop/Bridge Conformation Ratio on Elastic Properties of the Sphere-Forming ABA Triblock Copolymers under Uniaxial Elongation

Yoshiaki Takahashi,*,† Yihu Song,†,§ Norio Nemoto,†,‡ Atsushi Takano,‡ Yoshihiko Akazawa,‡ and Yushu Matsushita‡

Department of Molecular and Material Sciences, IGSES, Kyushu University, Kasuga, Fukuoka 816-8580, Japan, and Department of Applied Chemistry, Graduate School of Engineering, Nagoya University, Nagoya 464-8603, Japan

Received April 6, 2005; Revised Manuscript Received August 25, 2005

ABSTRACT: Elongational behavior of sphere-forming triblock copolymers is examined using a series of sample having almost the same molecular weight but different bridge fractions prepared by mixing polystyrene-*b*-polyisoprene-*b*-polystyrene (SIS) and the cyclic-SI. A polystyrene-*b*-polyisoprene-*b*-poly(2-vinylpyridine) sample was also used as a 100% bridged reference. The lattice deformation examined by SAXS can be well expressed by affine deformation, independent of the bridge fraction. Macroscopic stress and the orientation function of I segments examined by IR dichroism can be also approximately expressed by affine deformation, where magnitudes are proportional to the bridge fraction. In the stress−strain curves, small shoulders were observed at low strains. The presence of the shoulder can be explained by restoring force of the lattice, the magnitude of which depends on the regularity of the microdomain lattice. It is found that the restoring force linearly depends on the bridge fraction of the middle block chains in bulk states, in contrast to the results reported for solvent-containing systems.

Introduction

ABA triblock copolymers such as polystyrene-*b*-polyisoprene-*b*-polystyrene (SIS) and polystyrene-*b*-polybutadiene-*b*-polystyrene (SBS) are widely used in industries. For example, when polystyrene domains in the ordered states act as physical cross-linking points, these materials become typical thermoplastic elastomers. In such systems, rubbery middle block bridges two microdomains of polystyrene end blocks in the ordered states, giving characteristic rheological properties depending on morphology, middle block molecular weight, conformation of chains, and so on. There are significant numbers of studies concerning block copolymers so that they are frequently reviewed, and related references can be found in such articles.[1−5]

One of the main factors that influence the deformation mechanism of ABA triblock copolymers is the chain conformation of the middle block.[1] When both ends are anchored on the same A domain, a middle block possesses loop conformation, while when both ends are anchored on different A domains, a middle block possesses bridge conformation. Moreover, when AB diblock copolymer is contaminated, there exists a dangling end. The fraction of loop, bridge, and dangling end will significantly affect the rheological behaviors; thus, determination of their fractions and clarification of their roles in the deformation mechanism is one of fundamental issues in triblock copolymers.

Watanabe et al.[6−9] challenged this problem using SIS triblock copolymers with dipole-inverted polyisoprene chains. They determined the bridge fraction for lamellar-forming SIS triblock copolymer,[6] and the result was found to be consistent with a theoretical calculation.[10] In the subsequent studies,[7,9] the bridge fractions of sphere-forming SIS in an I-selective solvent and in low molecular weight I-homopolymer were determined with the same method. They reported that the contribution of osmotic constraint for loop chains in solution to the equilibrium elasticity of regularly arranged S domains is comparable to that of the bridge chains. The osmotic constraint becomes weaker in I-homopolymer.[7] Bridge fraction decreases with decreasing the concentration due to the stretching and destabilization of bridge conformation on dilution.[9]

Recently, Takano et al.[11] reported preparation and characterization of cyclic-SI diblock copolymers with different composition and studied their morphologies. Following the same procedures, sphere-forming cyclic-SI diblock copolymers are synthesized as reported in a previous paper.[12] They prepared a series of samples having almost the same size of spherical microdomains but different loop/bridge fractions by mixing the cyclic-SI and the original SIS used for the preparation of cyclic-SI. It was observed that the Young's moduli obtained by dynamic elongational measurements linearly increase with a decrease in the content of cyclic-SI. Using a polystyrene-*b*-polyisoprene-*b*-poly(2-vinylpyridine) (SIP) triblock copolymer, corresponding to the sample in which one of end S blocks is replaced to P, as a 100% bridged reference, they determined the bridge fraction of the I chains in SIS and SIS/cyclic-SI blends. Furthermore, it was reported that breaking stress of the samples obtained by uniaxial elongation at very fast velocity is proportional to the bridge fraction.[12]

In this paper, we further study the elongational behavior of such cyclic-SI containing SIS molecules reffering the results for SIP. The deformation of microdomain lattice is examined by small-angle X-ray scat-

† Kyushu University.
‡ Nagoya University.
§ Permanent address: Institute of Polymer compounds, Department of Polymer Science and Technology, Zhejiang University, Hangzhou 310027, China.
* Corresponding author: e-mail ytak@mm.kyushu-u.ac.jp; Ph +81-92-583-8822; Fax +81-583-8822.

10.1021/ma050720w CCC: $30.25
Published on Web 10/21/2005

Table 1. Young's Moduli and Bridge Fractions of the Samples

sample	ϕ_{bridge}	E'/MPa	sample	ϕ_{bridge}	E'/MPa
SIP	1	1.54	C25	0.63	1.02
SIS	0.93	1.43	C66	0.29	0.54
C13	0.73	1.18			

tering (SAXS) measurements, while macroscopic stress and deformation at the local segmental level are examined by measurements of simultaneous in-situ microscopic infrared dichroism and macroscopic stress under uniaxial elongation.

Experimental Section

The samples used are two kinds of triblock copolymers, i.e., SIP and SIS and blend samples from SIS and cyclic-SI diblock copolymer, used in the previous paper.[12] Number-averaged molecular weights of SIP and SIS are 13.5×10^4 and 14.7×10^4, respectively. The volume fraction of I component in all the samples is about 0.9. Among five blend samples used in the previous paper, C13, C25, and C66 (two-digit numbers show percentage of cyclic polymer) are used in the SAXS measurement while C25 and C66 are used in other measurements, due to the available amount of the samples. The bridge fraction ϕ_b in SIS, C13, C25, and C66 is 0.93, 073, 0.63, and 0.29, respectively.

SAXS measurement at room temperature was performed with Rigaku Nano Viewer equipped with a confocal max-flux mirror as a collimating system and an imaging plate as a 2-dimensional detector. The wavelength and the sample to the detector distance were 0.154 nm and 710 mm, respectively. X-rays were generated under the operating conditions of 45 kV/60 mA. To get rid of the effect of residual strain on the scattering data, hot-pressed films with thickness of about 1 mm were annealed at 110 °C for 3 days before the SAXS measurements. A homemade film stretching device was used to measure SAXS at constant strain whose magnitude was determined from direct measurement of film dimensions. It was confirmed from elongational stress measurements at the same conditions that stress relaxation during the SAXS measurements was negligible (maximum 10%).

Infrared dichroism and the macroscopic stress under uniaxial elongation at room temperature were measured with an instrument built by Shigematsu et al.[13] The basic part of this instrument is a Bio-Rad FTS 6000 FT-IR spectrometer, combined with an IR microscope equipped with a MCT detector. The sample cell is designed to perform stress measurements under uniaxial elongation. In this measurement, the dichroic ratio at elongation time t, $A(t) = A_{\parallel}(t)/A_{\perp}(t)$, where $A_{\parallel}(t)$ and $A_{\perp}(t)$ are absorbances of polarized IR parallel and perpendicular to the draw direction, respectively, is obtained. The dichroic ratio is related to the orientation function $f(t)$ by

$$f(t) = \langle 3\cos^2\theta(t) - 1\rangle/2 = [(A(t) - 1)/(A(t) + 2)]/[(A_0 - 1)/(A_0 + 2)]$$

where $\theta(t)$ is the orientation angle of the main chain respect to the draw direction and $A_0 = 2\cot^2\psi$ is the perfect dichroic ratio of a transition moment making an angle ψ with the direction of molecular main chain axis.[14] The setup details, measurement procedure, and performance of this instrument were reported elsewhere.[13]

Sample films are prepared by a hot-press at 150 °C for 5 min. A solution-cast film of SIP from dilute THF solution, annealed at 150 °C for 12 h, is also prepared. Hereafter, we simply call the hot-pressed film and the annealed solution-cast film as the pressed film and the annealed film, respectively. The thicknesses of the films were in the range between 30 and 50 μm. All films are carefully cut to a rectangular shape of 10 mm long and 3 mm wide for the measurements. The elongation rate was 0.1 mm/min. Absorption bands at 1004 cm^{-1} (C−C stretching),[15] 1602 cm^{-1} (benzene stretching),[16] and 1591 cm^{-1} (pyridine stretching)[17] are used to determine orientation functions in I, S, and P domains, respectively.

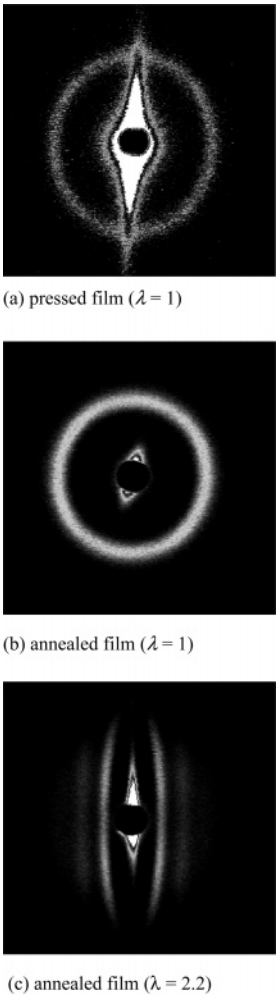

Figure 1. Examples of 2-dimensional SAXS pattern for SIS at different strains. The sample is elongated in the horizontal direction.

Results

Figure 1 shows examples of SAXS patterns obtained for the pressed and the annealed films at $\lambda = 1$ and at $\lambda = 2.2$ for the annealed film. It is clear that the observed pattern for the pressed film is anisotropic while that for the annealed film is isotropic, reflecting the effects of residual strain on the lattice structure in pressed film and their removal by annealing. The isotropic pattern observed for the annealed film becomes anisotropic when stretched. The intensity along the horizontal direction (stretching direction) becomes stronger, and peak positions move to a lower angle with an increase in λ. Higher order peaks become appreciable at high strains. On the other hand, the intensities along the vertical direction become weaker, and peak positions move to higher angle and disappears eventually. We analyzed these data by sector averaged intensity I (±10° arc) as a function of scattering vector $q = [4\pi \sin(\theta_S/2)]/\lambda_0$ along the stretching direction, where θ_S is the scattering angle and λ_0 the wavelength of incident X-ray. Along the vertical direction, the intensity was too weak for accurate data analysis.

Figure 2 compares examples of plots of I against q at three different strains. The data are vertically shifted to avoid overlapping. As mentioned above, peak posi-

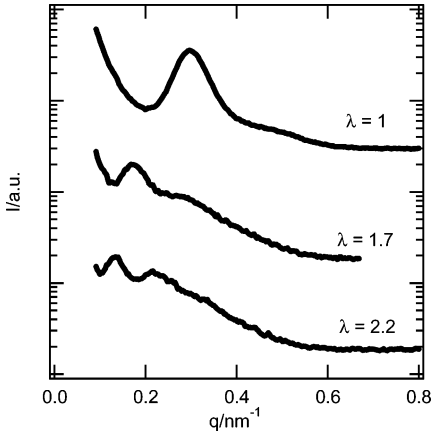

Figure 2. Sector averaged intensity (±10° arc) against wave vector for C66 at different strains. The strains are denoted in the figure.

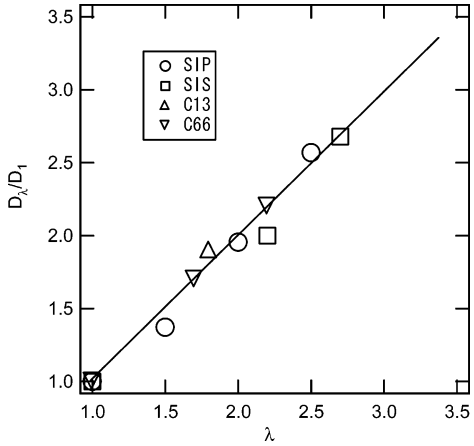

Figure 3. Strain dependence of the domain spacing in the elongation direction for SIP, SIS, C13, and C66. The symbols are denoted in the figure. The slope of solid line is 1.

tions move toward smaller q with increasing the strain, though the higher order peaks are not clearly seen. It should be noted that the domain spacing of linear and ring block copolymers having the same molecular weight and the same composition are different.[18] Therefore, domain spacing obtained from the first-order peak at deformed states, D_λ, were reduced using the respective values at rest, D_1, and plotted against strain in Figure 3. It is clear that all data fall on a straight line with slope 1, implying that all samples are affinely deformed at lattice level irrespective of the bridge fraction.

In the in-situ measurements of macroscopic stress and IR dicroism, changes in the width of the tested film observed by microscope and IR structural absorbance were consistent; that is, they showed the same macroscopic strain dependence under elongation. Thus, we could assume uniform deformation without the volume change and obtained true strain λ by $\lambda = (W/W_0)^{-2}$, where W is width of the film under elongation and W_0 is the initial width. Nominal stress σ_n is converted to the true stress by $\sigma = \sigma_n\lambda$.

Figure 4a shows true strain λ dependences of orientation functions f for S and P components (f_S and f_P) in SIP and C66 pressed films. Figure 4b compares f_I for I in the annealed and the pressed SIP films. No strain dependence was observed for f_S in C66, indicating that this hard domain does not deform during elongation. It is seen that f_P very slightly decreases with increasing λ. Moreover, in contrast to the f_S in C66, a continuous

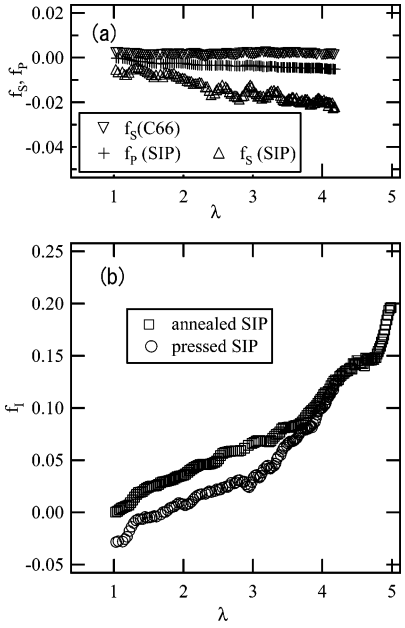

Figure 4. Strain dependence of orientation function for (a) S and P components in the SIP and C66 pressed films and (b) I component for annealed and pressed SIP films. Symbols are denoted in the figure.

decrease was observed for f_S in SIP. It should be noted that glass transition temperature T_g and its molecular weight dependence of S and P chains are similar;[19] however, they very weakly decrease in the order of S in ring, P in SIP, and S in SIP since the molecular weight of the former is about double the latter. Thus, the above differences in behavior of f can be attributed to the difference in decrease of T_g. S and P chains in SIP can slightly deform even at room temperature. However, the f_P value at $\lambda = 4$ is only about -0.005, which is negligibly small compared to the value for the full stretching (-0.5). The f_S value at $\lambda = 4$ is still about -0.02, which is also very small. Therefore, we conclude that the deformation of S and P is negligibly small compared to that of elastic I chains.

The orientation function f_I in Figure 4b for the pressed film starts from a nonzero value and steeply increases below $\lambda = 1.25$, and then it gradually but continuously increases with increasing the strain up to $\lambda = 3$. Since such offset and steep increase of f_I are not observed for the annealed film in the corresponding strain region, those observations can be attributed to the residual strain in pressed film observed in the SAXS pattern (Figure 1). In the middle range of strain (1.25−3) both data show almost the same strain dependence. At strains higher than 3, f_I for the pressed film increased more steeply than that for the annealed film up to $\lambda = 4.2$, the highest strain applied for the pressed film. In-situ microscopic observation of samples under deformation revealed that microcracks having a typical length of 10 μm start to develop at around strain of 2.5−3, which are more frequently observed in the annealed film than in pressed film, presumably resulting in the lower strain dependence of f_I for the annealed film.

Figure 5 compares true stress−strain (S−S) curves obtained for pressed and annealed films. For the annealed film, it is observed that σ increases somewhat steeply below $\lambda = 1.25$, followed by more mild increase of σ with increase of λ, resulting in a shoulder-like portion observed around $\lambda = 1.5$, which was not observed for f in Figure 4. Further scrutinized inspection

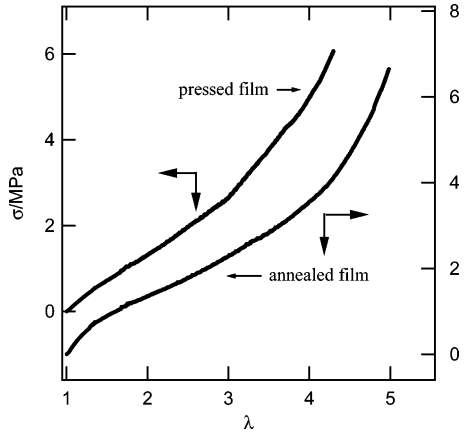

Figure 5. Comparison between stress−strain curves for the annealed and the pressed films for SIP.

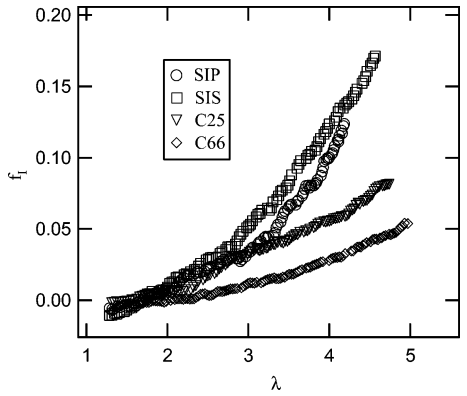

Figure 6. Strain dependence of orientation function for I segments in all samples. The samples are denoted in the figure.

reveals that there also exists a tiny shoulder in the S−S curve of the pressed film (which will be shown more clearly in Figure 7b). Since the effects of residual strain should be larger for the pressed film than the annealed film, the existence of the shoulder in the S−S curves cannot be attributed to the residual strain. The effect of the residual strain may be minor for the S−S curves. The stress σ of the pressed film tends to increase more rapidly compared with that of the annealed film at higher strains ($\lambda = 2-5$), which may reflect generation of microcracks in referring to the discussion of the λ dependencies of the orientation function shown in Figure 4. For a pressed SIP film, reversal and repeated measurements are also performed. The data coincided with each other when the applied strain was small (up to $\lambda = 3$), while the reproducibility of the data became poor when high strain was applied. In the latter case, it was observed that the stress does not increase with strain up to say $\lambda = 1.2$, which may be attributed to the microcracks generated in the prior measurement with high strain.

Figures 6 and 7a respectively show plots of orientation function f_I and macroscopic stresses σ against strain λ for all the pressed films. In Figure 6, data at $\lambda < 1.25$ are omitted since they are influenced by the residual strain. As shown in Figure 3, SAXS data (lattice deformation) can be well represented by affine deformation up to $\lambda = 3$. Thus, it is expected that f_I and σ can be also expressed by the affine deformation, at least up to $\lambda = 3$. We first test this idea for σ data because of more smooth variations in σ with λ compared with the variation of f_I. As mentioned above, there exists a

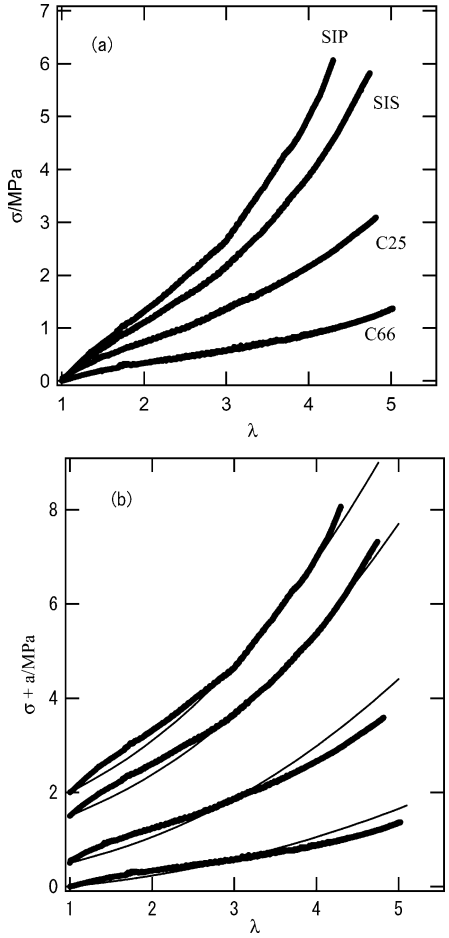

Figure 7. (a) Stress−strain curves for all samples. The samples are denoted in the figure. (b) Comparison between the experimental data in (a) and the fitted affine deformation (thin solid lines). The data for SIP, SIS, C13, and C25 are vertically shifted by factors of 2, 1.5, 1, and 0.5, respectively, to avoid overlapping.

shoulder in the S−S curve for SIP at $\lambda < 2.5$ (Figure 5), which may also exist for other samples. The effect of microcrack generation, which was apparent for the f_I of the annealed film at $\lambda > 3$, may influence the data at higher strains. Nonlinear effects for bridged chains and small contribution of looped chains to the stress are expected at high strains, but contribution of looped chains to the stress at low strains is unknown. To avoid the effects of these factors and to clarify the characteristics of S−S curves, fitting to the affine deformation ($\sigma = G(\lambda^2 - \lambda^{-1})$, where G is a fitting parameter) at around $\lambda = 2.5-3.5$, as shown by thin solid lines in Figure 7b. It is clear that the shoulder exists in the S−S curve for SIP and SIS below $\lambda = 2.5$, while the data can be well represented by the affine deformation up to, say, $\lambda = 4$, but the data deviate upward from the affine deformation line at the high strain end denoting the nonlinear effects. On the other hand, the coincidence of σ data and the affine deformation line seems to be poor for the samples containing cyclic polymer; their validity will be shown later (Figure 10). Thus, we can point out that there also exists shoulder in the S−S curve for these samples, which shall be discussed later. The downward deviation of the data from fitted lines at high strains for the samples containing cyclic polymer can be attributed to the microcrack generation.

It is clear in Figures 6 and 7a that f_I and σ are higher for samples with higher bridge fraction ϕ_b. These data

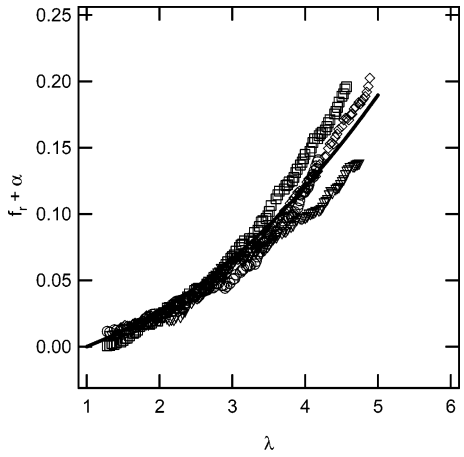

Figure 8. Reduced plots of the orientation function shown in Figure 6. Symbols are the same as those in Figure 6. The solid line denotes affine deformation.

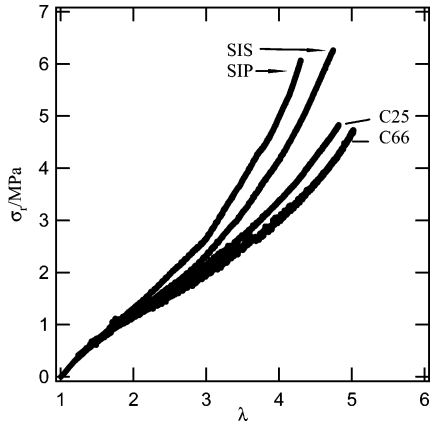

Figure 9. Reduced plots of the stress−strain curves shown in Figure 7. The samples are designated in the figure.

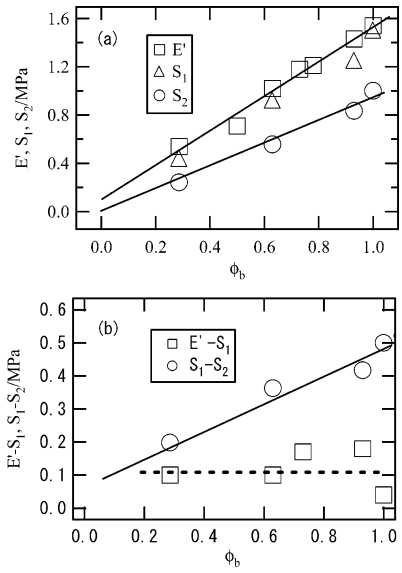

Figure 10. (a) Plots of E', S_1, and S_2 against bridge fraction ϕ_b and (b) $E' - S_1$ and $S_1 - S_2$ against ϕ_b. The symbols are denoted in the figure.

are reduced by the bridge fraction as $f_r = f_1/\phi_b$, $\sigma_r = \sigma/\phi_b$ and plotted against strain in Figures 8 and 9, respectively. In Figure 8, f_r data for each sample are slightly shifted in the vertical direction by the factor of α (ranging from 0.005 to 0.02) to remove the offset. Most of the data in Figure 8 approximately compose a single line along the affine deformation line (solid line) up to $\lambda = 3.5$. In Figure 9, σ_r data for SIP are slightly higher than others. However, the difference is not so significant up to $\lambda = 3.5$ and can be approximately represented by affine deformation as already shown in Figure 7b. Thus, both f and σ can be approximately represented by affine deformation, and their magnitudes are proportional to the bridge content in that strain region. At higher strains, it is clear that the stress data become lower with decreasing the bridge fraction, implying that the microcrack generation becomes more frequent with decrease of ϕ_b.

Discussion

Prasman and Thomas[20] and Daniel et al.[21] studied deformations of sphere-forming A−B−A triblock copolymers under simple elongation up to $\lambda = 3$ by SAXS and by small-angle neutron scattering (SANS) up to $\lambda = 3.5$, respectively. They reported that lattice deformation is affine, whereas macroscopic stress is nonaffine. Therefore, our SAXS data are consistent, but the stress data are not consistent with their results since our data can be represented by the affine deformation, though there is a small shoulder at low strains. In this connection, it may be noted that if the shoulder in our S−S curves become much larger, the profiles become similar to the corresponding figures reported by Prasman and Thomas[20] and Daniel et al.[21] In other words, the shoulder of the S−S curve in their data are extremely large and extended to somewhat larger strain than those observed in Figures 5 and 7. This suggests that the discrepancy of their data and our data might be attributed to the magnitude of the shoulder, which can be explained by restoring force of regularly arranged lattice mentioned below.

According to Watanabe et al.,[7,9,22] elastic behaviors of the systems containing spherical domains (sphere-forming SIS triblock and SI diblock in an I-selective solvent, SIS in low molecular weight homo-I)[7,9] or particles (concentrated spherical silica suspensions in Newtonian media)[22] are enhanced by restoring force against deformation of the regularly arranged isotropic lattice formed by the spherical domains or the particles. That is, when the lattice is slightly deformed, restoring force to the stable position of the lattice is generated. The magnitude of restoring force depends on the regularity of the lattice, which may become the highest for the perfect lattice. When relatively large strain is applied to the system, the lattice is disrupted and such restoring force disappears.[23]

If the restoring force of the lattice may give rise to the shoulder in S−S curves, the difference in the magnitude of the shoulders observed between the pressed film and the annealed film in our study (Figure 5) is consistent with the fact that the latter has higher regularity of the lattice. Large shoulders reported by Prasman and Thomas[20] and Daniel et al.[21] are also reasonable since the sample in the former study contains mineral oil (selective solvent for the middle block), while the lattice in the sample in the latter study is well arranged as shown by their SAXS data.

It has been reported that the restoring force is independent of bridge fraction.[7,9] To examine this, we analyzed two slopes, S_1 and S_2, of the S−S curve. Here, the slope S_1 is the initial slope of the experimental data shown in Figure 7, which must be equal to Young's modulus. The slope S_2 is the initial slope of fitted affine

deformation lines shown in Figure 7b, which corresponds to the hypothetical Young's modulus without the contribution of the restoring force. Since the fitting was carried out in a narrow strain range, estimated S_2 may contain certain ambiguities, but we think these slopes are accurate enough to discuss semiquantitatively the bridge fraction dependence of the magnitude of the shoulders.

Figure 10a shows bridge fraction ϕ_b dependencies of S_1 and S_2, together with E' data, which were measured for annealed samples (annealed at 150 °C for 12 h) by dynamic elongational measurements (at 70 °C, 10 rad/s).[12] Three sets of data are proportional to the bridge fraction. At the each bridge fraction, E' value measured for the annealed sample is always the highest, while S_2 is the lowest, consistent with the above idea. That is, the modulus becomes larger when the sample is close to the equilibrium state (E' of the annealed film) than that having somewhat irregular arrangement of spherical domains (S_1 of the pressed film). The difference between E' and S_1 reflects the effects of annealing and the difference between S_1 and S_2 corresponds to the restoring force for the pressed sample. Figure 10b shows the bridge fraction dependencies of $E' - S_1$ and $S_1 - S_2$. Since $E' - S_1$ values are almost constant, we conclude that the annealing effects is independent of the bridge fraction. It is also clear that $S_1 - S_2$ linearly increases with an increase of the bridge fraction. This result implies that the restoring force depends on the conformation of middle block chains in bulk states, in contrast to the results reported for the solvent-containing systems, in which restoring force was independent of the chain conformation.[7,9]

Richards and Welsh[24] examined chain dimension of I chain of sphere-forming SIS under uniaxial elongation by SANS. They reported that the chain dimension along the stretching direction is larger than the value expected from affine deformation, while it is smaller than the expected value along the perpendicular direction. They tentatively attributed the enhanced anisotropy of the chain dimension to the displacement of relatively large S domains. At present, we speculate that the restoring force may be originated from such direction-dependent nonaffine deformation of middle I chains, which may be different for bridge and loop chains resulting in the bridge fraction dependence of restoring force. Further studies on the anisotropy of chain dimensions for the samples with different loop/bridge fraction are needed to clarify the above speculations.

Conclusions

We examined elongational behavior of sphere-forming triblock copolymers having different bridge fractions prepared by mixing polystyrene-*b*-polyisoprene-*b*-polystyrene triblock copolymer (SIS) and the end-linked cyclic-SI diblock copolymer. A polystyrene-*b*-polyisoprene-*b*-poly(2-vinylpyridine) sample was also used as a 100% bridged reference. The lattice deformation examined by SAXS for $\lambda < 3$ can be well expressed by affine deformation, independent of the bridge fraction. Macroscopic stress and the orientation function of I segments examined by IR dichroism can be also approximately expressed by affine deformation, and their magnitudes are proportional to the bridge fraction of the samples up to $\lambda = 3.5$. In the stress−strain curve, small shoulder-like enhancement of the stress was observed at low strains. The magnitude of the shoulder depends on the preparation condition of sample films, that is, the regularity of the microdomain lattice. The existence of such a shoulder can be explained by restoring force of lattice, already known for other lattice-forming systems. It is found that the restoring force in bulk states linearly depends on the bridge fraction of middle block chains, in contrast to the results for solvent-containing systems.

References and Notes

(1) Watanabe, H. In *Structure and Properties of Multiphase Polymeric Materials*; Araki, T., Qui, T. C., Shibayama, M., Eds.; Marcel Dekker: New York, 1998; Chapter 9.
(2) Spontak, R. J.; Patel, N. P. *Curr. Opin. Colloid Interface Sci.* **2000**, *5*, 334−341.
(3) Hamley, I. W. *Curr. Opin. Colloid Interface Sci.* **2000**, *5*, 342−350.
(4) Hamley, I. W. *J. Phys.: Condens. Matter* **2001**, *13*, R643−R671.
(5) Lodge, T. P. *Macromol. Chem. Phys.* **2003**, *204*, 265−273.
(6) Watanabe, H. *Macromolecules* **1995**, *28*, 5006−5011.
(7) Watanabe, H.; Sato, T.; Osaki, K.; Yao, M.-L.; Yamagishi, A. *Macromolecules* **1997**, *30*, 5877−5892.
(8) Watanabe, H.; Sato, T.; Osaki, K.; Matsumiya, Y.; Anastasiadis, S. H. *Nihon Reoroji Gakkaishi* (*J. Soc. Rheol. Jpn.*) **1999**, *27*, 173−182.
(9) Watanabe, H.; Sato, T.; Osaki, K. *Macromolecules* **2000**, *33*, 2545−2550.
(10) Zulina, E. B.; Halperin, A. *Macromolecules* **1992**, *25*, 5730−5741.
(11) Takano, A.; Kadoi, O.; Hirahara, K.; Kawahara, S.; Isono, Y.; Suzuki, J.; Matsushita, Y. *Macromolecules* **2003**, *36*, 3045−3050.
(12) Takano, A.; Kamaya, I.; Takahashi, Y.; Matsushita, Y. *Macromolecules* **2005**, *38*, 9718−9723.
(13) Shigematsu, Y.; Takada, A.; Nemoto, N.; Nitta, K. *Rev. Sci. Instrum.* **2001**, *72*, 3927−3932. Song, Y.; Shigematsu, Y.; Nitta, K.; Nemoto, N. *Polym. J.* **2002**, *34*, 584−592.
(14) Siesler, H. W. *Adv. Polym. Sci.* **1981**, *65*, 1.
(15) Arjunan, V.; Subramanian, S.; Mohan, S. *Spectrochim. Acta, Part A* **2001**, *57*, 2547−2554.
(16) Liang, C. Y.; Koenig, J. L. *J. Polym. Sci.* **1958**, *27*, 241−254.
(17) Cester, L. C.; Meaurio, E.; Katime, I. *Macromolecules* **1993**, *26*, 2323−2330.
(18) Matsushita, Y.; Iwata, H.; Asari, T.; Uchida, T.; ten Brinke, G.; Takano, A. *J. Chem. Phys.* **2004**, *121*, 1129−1132.
(19) Takahashi, Y.; Ochiai, N.; Matsushita, Y.; Noda, I. *Polym. J.* **1996**, *28*, 1065−1070. Takahashi, Y.; Kitade, S.; Noda, M.; Ochiai, N.; Noda, I.; Imai, M.; Matsushita, Y. *Polym. J.* **1998**, *30*, 388−393.
(20) Prasman, E.; Thomas, E. L. *J. Polym. Sci., Part B: Polym. Phys.* **1998**, *36*, 1625−1636.
(21) Daniel, C.; Hamley, I. W.; Mortensen, K. *Polymer* **2000**, *41*, 9239−9247.
(22) Watanabe, H.; Yao, M.; Yamagishi, A.; Osaki, K.; Shikata, T.; Niwa, H.; Morishima, Y. *Rheol. Acta* **1996**, *35*, 433−445.
(23) Tan, H.; Watanabe, H.; Matsumiya, Y.; Kanaya, T.; Takahashi, Y. *Macromolecules* **2003**, *36*, 2886−2893.
(24) Richards, R. W.; Welsh, G. *Eur. Polym. J.* **1995**, *31*, 1197−1206.

MA050720W